Wavelength dependence of optical tweezer trapping forces on dye-doped polystyrene microspheres

M. J. Kendrick,* D. H. McIntyre, and O. Ostroverkhova

Department of Physics, Oregon State University, Weniger Hall 301, Corvallis, Oregon 97331-6507, USA
**Corresponding author: kendricm@onid.orst.edu*

Received June 26, 2009; accepted August 26, 2009;
posted September 16, 2009 (Doc. ID 113368); published October 30, 2009

We present an experimental and numerical study of the wavelength dependence, near resonance, of the optical tweezer trap stiffness on three different dye-doped 1 μm polystyrene spheres with peak absorptions at $\lambda = 625$, 775, and 840 nm. Experimentally, an increase in the trap stiffness of ~35% on the red side of resonance was observed for the dye-doped spheres relative to polystyrene spheres without dye. Numerical simulations for spheres of different sizes, between 20 nm and 1 μm, and for absorption strengths corresponding to peak extinction coefficient values between 0.0027 and 0.081 were also conducted. Numerical results showed a maximum increase in the trap stiffness of ~35%, which is consistent with experimental results. © 2009 Optical Society of America

OCIS codes: 140.7010, 160.4760.

1. INTRODUCTION

Since 1970 optical traps have been used to confine and manipulate particles for applications in chemistry, biology, engineering, and physics [1]. In particular, single-beam gradient traps, referred to as optical tweezers, have been used to manipulate micrometer-sized dielectric particles, which can be trapped with low- to moderate-power lasers. Optical tweezers with particles on this size scale have been used in experiments that include observing mechanical properties of DNA [2], measuring forces produced by molecular motors [3], micromachining, and assembling both ordered arrays and 3D structures of particles [4]. However, experiments done with nanometer-sized particles, or "nanoparticles," are limited [5,6]. Given the recent emphasis on nanotechnology and the desire to design experiments on the nanoscale, there is motivation to trap and manipulate particles on this scale. Furthermore, the ability to not only confine nanoparticles but to further suppress their natural Brownian motion to the nanometer and subnanometer scales is desirable. One possible application is a nanometer-sized fluorescent probe for biological experiments. Such an application would require spatial control of the nanometer-sized probe with a high precision without using large laser powers to avoid damaging the object under observation. However, adapting optical tweezers for applications on the nanoscale is difficult because the trapping force on nanoparticles scales with the volume of the particle [6]. Thus, under the same conditions, the force acting on a 1 nm particle is 10^6 times smaller than the force on a 100 nm particle.

A possible method to increase the trapping force exerted on nanoparticles would be to exploit optical resonances. For example, atoms, on the subnanometer scale, have been successfully trapped using optical tweezers [7]. The reason that atoms can be trapped is that the wavelength of the trapping laser can be tuned close to a strong resonance transition where the optical response of the atom is enhanced. However, resonances in transparent dielectric spheres are in the ultraviolet, far from the typical near-infrared wavelengths used in optical tweezers. Potential candidates for resonance-enhanced optical trapping include metallic nanoparticles, metal–dielectric nanoshells, quantum dot nanocrystals, chromophore-doped nanoshells, dye-doped dielectric particles, and carbon nanotubes. In all of these cases, we can tune the laser wavelength to match the optical response and thus enhance the optical forces. An even more exciting prospect is that in many cases we can tune the particle's optical response through synthesis to a range of wavelengths that includes a desired trapping wavelength [8–12].

To explore the possibilities of resonance-enhanced optical trapping, we have conducted experiments with polystyrene spheres doped with various dyes and performed numerical calculations of the trapping forces. The aim of these experiments and calculations is to study the additional force contributions from the resonance of the dye that is added to spheres, in particular, the wavelength dependence. These spheres are a model system to quantitatively explore this resonance effect on the trapping force as they have been used extensively in optical tweezers, and the forces on transparent polystyrene spheres are well understood. Our experimental and numerical results suggest, however, that a dye resonance does not provide a significant increase in the trapping force at wavelengths near resonance.

2. THEORY

The force acting on a particle in an optical tweezer trap is a result of the transfer of momentum between the highly

focused laser light and the particle. The forces acting on a spherical particle of arbitrary size can be determined analytically using electromagnetic (EM) scattering theory. For spherical particles much smaller or much larger than the wavelength of the trapping light, approximations can be applied to make the calculation of the trapping force less intensive. In addition, when using these approximations to calculate the trapping force ($\boldsymbol{F}_{trap}$) it is possible to separate the force into three components: the scattering force ($\boldsymbol{F}_{scat}$), the absorption force ($\boldsymbol{F}_{abs}$), and the gradient force ($\boldsymbol{F}_{grad}$), where $\boldsymbol{F}_{trap}=\boldsymbol{F}_{grad}+\boldsymbol{F}_{scat}+\boldsymbol{F}_{abs}$ [13]. The gradient force attracts the particle toward the high intensity focus of the trap, to trap the particle, and acts as a restoring force when the particle is displaced from equilibrium. The scattering and the absorption forces act in the direction of propagation of the laser, pushing the particle away from the high intensity focus. If the scattering and the absorption forces exceed the gradient force, it is not possible to trap the particle in three dimensions [14]. When performing calculations using rigorous EM theory, the trapping force cannot be easily separated into the scattering, absorption, and gradient forces, but qualitatively the gradient of the field traps the particle, while scattering and absorption destabilize the trap.

A. Optical Tweezer Force on an Arbitrarily Sized Sphere

To calculate the forces acting on an arbitrarily sized sphere, the EM scattering theory must be employed to determine the EM fields scattered from the sphere in the trap. The Lorentz–Mie theory can be used to obtain an analytical solution of the scattered fields from a sphere, given an incident plane wave EM radiation [15,16]. However, optical tweezers are created using highly focused light. Several techniques have been developed to extend the Lorentz–Mie theory to fields scattered from a sphere with arbitrary incident EM fields, including the generalized Lorentz–Mie theory (GLMT) and the *T*-matrix method [17].

In the case of optical tweezers, the incident EM field is typically a highly focused Gaussian-profiled, or TEM_{00}, laser beam. A significant amount of research has been conducted on calculating the EM fields and forces in optical tweezers acting on a spherical particle using the GLMT and the *T*-matrix methods [18,19]. In both these methods, the incoming highly focused Gaussian field is expressed as an expansion of vector spherical wave functions (VSWFs), which are functions of spherical Bessel functions [20]. The expansion coefficients of the VSWFs that define the fields of the incoming Gaussian beam are determined using a point matching algorithm in the far field [21]. The EM field scattered from the particle (i.e., outgoing field) can then be determined from the incoming field using the *T*-matrix method [17]. For example, Nieminen *et al.* [22] presented the incoming and outgoing fields ($\boldsymbol{E}_{\text{in}}$ and $\boldsymbol{E}_{\text{out}}$, respectively) in terms of the VSWF and expansion coefficients as follows:

$$\boldsymbol{E}_{\text{in}}=\sum_{i=1}^{\infty}\sum_{j=-i}^{i} a_{ij}\boldsymbol{M}_{ij}^{(2)}(k_m\boldsymbol{r})+b_{ij}\boldsymbol{N}_{ij}^{(2)}(k_m\boldsymbol{r}), \tag{1}$$

$$\boldsymbol{E}_{\text{out}}=\sum_{i=1}^{\infty}\sum_{j=-i}^{i} p_{ij}\boldsymbol{M}_{ij}^{(1)}(k_m\boldsymbol{r})+q_{ij}\boldsymbol{N}_{ij}^{(1)}(k_m\boldsymbol{r}), \tag{2}$$

where $k_m=2\pi/\lambda_m$ is the wavenumber in the surrounding medium; $\boldsymbol{r}$ is the position vector; $\boldsymbol{M}_{ij}^{(l)}$ and $\boldsymbol{N}_{ij}^{(l)}$ are the VSWFs; and a_{ij}, b_{ij}, p_{ij}, and q_{ij} are the expansion coefficients. With expressions for the incoming and outgoing EM fields—given by Eqs. (1) and (2), respectively—the forces acting on the sphere in the Gaussian beam can be calculated by evaluating the momentum transfer from the EM fields to the particle, because the change in momentum of the particle must equal the change in momentum of the fields. This change in momentum, and thus the trapping force, can be calculated by taking a surface integral of the Maxwell stress tensor over a spherical surface in the far field. In particular, the force acting in the direction parallel to the propagation of laser light (taken here as the z direction) in SI units is [23]

$$\begin{aligned}F_z=&\frac{2n_m}{c}\sum_{i=1}^{\infty}\sum_{j=-i}^{i}\frac{j}{i(i+1)}\text{Re}(a_{ij}^{*}b_{ij}-p_{ij}^{*}q_{ij})\\&-\frac{1}{i+1}\left[\frac{i(i+2)(i-j-1)(i+j+1)}{(2i+1)(2i+3)}\right]^{1/2}\text{Re}(a_{ij}a_{i+1,j}^{*}\\&+b_{ij}b_{i+1,j}^{*}-p_{ij}p_{i+1,j}^{*}+q_{ij}q_{i+1,j}^{*}),\end{aligned} \tag{3}$$

where n_m is the index of refraction of the surrounding medium and c is the speed of light. The forces in the transverse direction (i.e., x and y directions) are obtained using the same expressions for the EM fields [Eqs. (1) and (2)] by rotating the coordinate system and defining new coefficients a_{ij}, b_{ij}, p_{ij}, and q_{ij} in the rotated frame of reference [19,24]. In the two limiting cases, $d\gg\lambda$ and $d\ll\lambda$, where d is the sphere diameter and λ is the wavelength of the trapping light, the expressions for the trapping force are simplified as described below.

1. Geometric Optics Regime ($d\gg\lambda$)

In the geometric optics regime ($d\gg\lambda$), the focused light that creates the optical tweezer trap can be described as an infinite number of rays that are incident on, and interact with, the particle at different angles, where the range of angles is determined by how strongly the light is focused. When each ray strikes the surface of the sphere, a portion of the light is scattered, a portion is absorbed, and a portion is transmitted. The relative amplitudes of the light that is scattered, transmitted, or absorbed depend on the index of refraction of the particle. The light that is reflected and absorbed by the sphere results in radiation pressure, or the scattering and absorption forces that act in the direction of propagation of the light. The transmitted light is refracted, resulting in a change in momentum as it enters and exits the sphere, which—according to Newton's third law—imparts an equal and opposite change in momentum to the particle. This change in momentum resulting from the refraction of the transmitted light is proportional to the force that confines the sphere and is referred to as the gradient force. In the geometric optics regime, a concise form of the total force (combining scattering and gradient forces) acting on a dielectric sphere when in an optical trap has been given by Ashkin

[25]. The expressions for the force in [25] show that rays incident at large angles contribute more to the gradient (and thus the trapping) force than those incident at small angles, with a maximum contribution from rays incident at an angle near 70° [26]. This dictates the choice of high numerical aperture (NA) objectives for optical tweezer traps.

2. Rayleigh Regime ($d \ll \lambda$)

In the Rayleigh regime ($d \ll \lambda$), the reaction of the particle to the incident EM field at any instant in time is approximately constant throughout the particle. The particle can then be approximated as a point dipole. In this regime, the trapping force acting on the dipole can succinctly be broken up into three components: the scattering, the absorption, and the gradient forces. In the case of a sphere, the scattering and absorption forces ($\boldsymbol{F_{scat}}$ and $\boldsymbol{F_{abs}}$, respectively) acting on the particle in the trap are [6]

$$\boldsymbol{F_{scat}} = \hat{\boldsymbol{k}}\left(\frac{n_m}{c}\right)C_{scat}I = \hat{\boldsymbol{k}}\frac{4\pi^3 n_m}{c\varepsilon_o^2\lambda^4}|\alpha|^2 I, \tag{4}$$

$$\boldsymbol{F_{abs}} = \hat{\boldsymbol{k}}\left(\frac{n_m}{c}\right)C_{abs}I = \hat{\boldsymbol{k}}\frac{2\pi}{c\varepsilon_o\lambda}[\mathrm{Im}(\alpha)]I, \tag{5}$$

where C_{scat} and C_{abs} are the scattering and absorption cross sections, ε_o is the dielectric constant in vacuum, α is the complex polarizability of the sphere, $\hat{\boldsymbol{k}}$ is the unit vector in the direction of propagation of the laser beam, and I is the intensity of trapping light. The polarizability of the sphere is related to the index of refraction by the Clausius–Mossotti equation (in SI units) [27],

$$\alpha = 4\pi\varepsilon_m\left(\frac{d}{2}\right)^3\left(\frac{m^2-1}{m^2+1}\right), \tag{6}$$

where ε_m is the dielectric constant, in SI units, of the surrounding material and m is the relative complex index of refraction, which is the ratio of the index of refraction of the sphere (n_s) to the index of refraction of the surrounding medium (n_m). The third force acting on the sphere is the gradient force $\boldsymbol{F_{grad}}$ [28],

$$\boldsymbol{F_{grad}} = \frac{\mathrm{Re}(\alpha)}{cn_m\varepsilon_o}\nabla I. \tag{7}$$

The trapping force on the sphere is the vector sum of $\boldsymbol{F_{grad}}$, $\boldsymbol{F_{scat}}$, and $\boldsymbol{F_{abs}}$. In the Rayleigh regime, the scattering force, which depends on the volume of the particle squared, is small compared with the gradient force, which depends on the volume [Eqs. (4), (6), and (7)]. Furthermore, it can be seen from Eqs. (5)–(7) that an increase in the trapping force can be obtained if the polarizability can be adjusted such that there is an increase in the real part of the polarizability, and hence $\boldsymbol{F_{grad}}$, without a substantial increase in the imaginary part, and $\boldsymbol{F_{abs}}$.

B. Resonant Enhancement of Optical Tweezer Trapping Force

Regardless of the sphere size, the force acting on a trapped particle depends on the complex index of refraction of the material. The real part of the index of refraction, the refractive index n, is attributed to reflection and refraction; and the imaginary part, the extinction coefficient κ, is attributed to absorption [29]. The behavior of the complex index in the vicinity of a resonance is illustrated in Fig. 1(a), which was calculated using the classic electron oscillator model [30]. The corresponding polarizability of a sphere with a diameter of 50 nm is calculated using Eq. (6) and is shown in Fig. 1(b). On the red side of resonance (e.g., >790 nm in Fig. 1) the increase in the real part of the polarizability exceeds the increase in the imaginary part so that the increase in the gradient force due to resonance is larger than the increase in the absorption force, resulting in an enhancement in the trapping force.

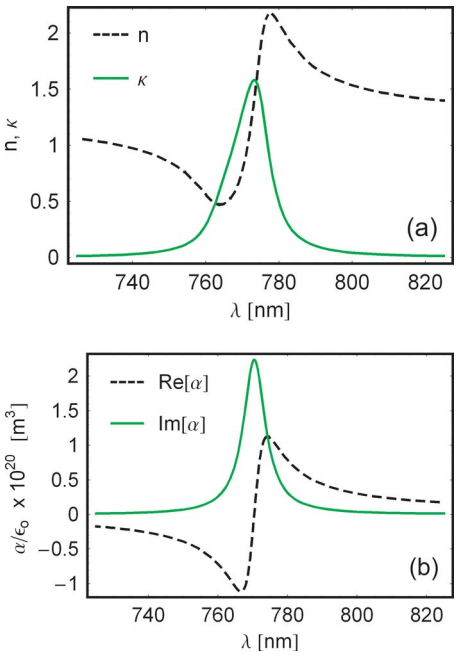

Fig. 1. (Color online) (a) Real and imaginary parts (n and κ, respectively) of the complex index of refraction near resonance, obtained from the classic electron oscillator model of the dielectric constant. (b) The real and imaginary parts of the polarizability, α in units of meters cubed near resonance, calculated using the complex index of refraction in (a), and the Clausius–Mossotti equation [Eq. (6)]. Both (a) and (b) show that there is an increase in either the real part of the index of refraction (i.e., in the refractive index n) or the real part of the polarizability on the red side of the resonance, which can be related to the forces acting on a particle in an optical trap.

Enhancement in the gradient force on the red side of an optical resonance has been exploited in the past to trap atoms and molecules on the subnanometer scale [7,31]. More recently, plasmon resonant particles ranging in size from 18 to 254 nm have been trapped experimentally with optical tweezers at wavelengths on the red side of resonance [14,32,33]. The applicability of the enhancement of the trapping force on nanometer-sized nonmetallic absorbing spheres has previously been explored theoretically, and the possibility of up to an order of magnitude increase was predicted [34].

3. EXPERIMENTAL

To quantitatively explore the wavelength dependence of optical forces in the vicinity of a resonance we have con-

ducted experiments using 1 μm polystyrene spheres doped with dye. We used micrometer-sized spheres because they are widely used in many optical tweezer applications, and techniques for trapping and measuring the optical trapping force on them are well documented [13,35,36]. In our experiments we measured the trapping force at multiple wavelengths near the dye resonance. As a control, similar measurements were taken on spheres without dye.

The dyed particles used in our experiments had peak absorption at wavelengths close to the tunability range of the trapping laser. The three types of particles we used were all 1 μm in diameter and had peak absorption at wavelengths of 625 (Crimson Spheres, Molecular Probes, Inc.), 775 (Duke Scientific, Inc.), and 840 nm (Duke Scientific, Inc.), later referred to as "625," "775," and "840 nm" spheres, respectively. We independently measured the extinction spectra of dyes used in the 775 and 840 nm spheres after extracting the dye from the spheres by dissolving them in acetone and filtering the solution using a 200 nm pore. The extinction spectra in Fig. 2 show that the dyes used in the 775 and 840 nm spheres have peak absorption in acetone at 760 and 825 nm, respectively. The inset in Fig. 2 shows the extinction spectrum of the 840 nm spheres in a de-ionized water (Di$-H_2O$) suspension. The spectrum of the dye-doped spheres is redshifted by ~15 nm and broadened, as compared with that of the dilute solution of the same dye in acetone (Fig. 2), due to aggregation effects. Similar effects were observed in the 775 nm spheres as well. We also verified that the dye was loaded in the spheres, and not in the solution, by filtering the dye-doped spheres from their Di$-H_2O$ suspensions using a filter with a 200 nm pore size. Extinction spectra measurements of the solutions were then taken before and after filtering. The spectral data suggested that no discernible amount of dye existed in the solution. Polystyrene spheres with a diameter of 1 μm without dye (transparent) from Duke Scientific, Inc. were also used as a control. All spheres were obtained from the manufacturer as a suspension in Di$-H_2O$ at concentrations between 2% and 10% by weight. These suspensions were ultrasonicated and further diluted with Di$-H_2O$ so that measurements could be taken without multiple spheres falling into the trap at the same time. Sample solutions were held between a microscope slide and a coverslip in a securely sealed fluid chamber.

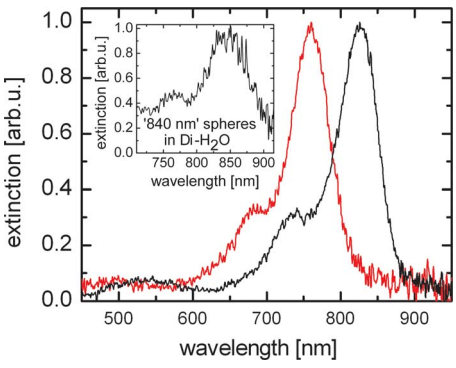

Fig. 2. (Color online) Extinction spectra of the dyes used in the 775 and 840 nm spheres in a dilute acetone solution, with peak absorption at 760 and 825 nm, respectively. The inset shows the spectrum of a Di$-H_2O$ suspension of the 840 nm spheres, which has a broadened peak that is redshifted by ~15 nm, as compared with the same dye in the acetone solution.

Optical tweezer trapping was performed in a custom inverted microscope assembly with an oil immersion microscope objective (Edmund Optics, 100×, NA of 1.25) as shown in Fig. 3. Particles were trapped with either a continuous wave (cw) Ti:sapphire laser, tunable between 750 and 840 nm, or a diode laser (λ=980 nm). The objective was placed on a 1D stage (z direction) to control the position of the trap in the sample. The sample was placed on a 2D stage (x and y directions) to control the trap position in the plane of the sample. For trap strength measurements, a helium–neon laser (633 nm) and Hamamatsu S4349 quadrant photodiode (QPD) were used to measure scattered light from the sphere undergoing Brownian motion in the trap [37]. The QPD signal was collected using a data acquisition card (DAQ) (NI-6221), and data acquisition was done using a custom LabView program. A halogen lamp and a CCD camera were used to illuminate the sample and image particles.

For our measurements we define the z direction as the direction of propagation of the laser beam and the x and y directions as transverse to the propagation. To measure the trap strength in the x direction the time series of the particle undergoing Brownian motion within the trap was acquired [Fig. 4(a)] and analyzed. In our analysis, we assumed that the trapping laser beam had a Gaussian spatial profile resulting in a Hooke's law restoring force, $F_{trap\ x}\hat{\boldsymbol{x}}=-k_x x\hat{\boldsymbol{x}}$, acting on the particle when it is displaced small distances x from equilibrium in the trap, where k_x is the trap stiffness (or the trap strength) and $\hat{\boldsymbol{x}}$ is the unit vector in the x direction. To support the validity of experimental results, we applied more than one data analysis technique to determine the trap stiffness. These included using the variance of the particle's motion in the trap [Fig. 4(a)] and the equipartition theorem, a Gaussian fit to a histogram of the distribution of the particle's fluctuations within the trap, and the corner frequency of the

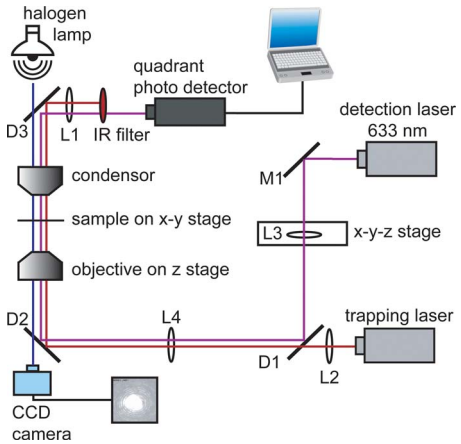

Fig. 3. (Color online) Experimental setup used to measure optical tweezer trap strength. Optical tweezer trapping was achieved by focusing either cw Ti:sapphire laser light (tunable between 750 and 840 nm) or diode laser light (980 nm) with a high NA objective. A detection laser (He–Ne) and a quadrant photodetector were used to measure the suppressed Brownian motion of a particle in the trap, from which the trap strength can be obtained. Notations: L, lenses; D, dichroic mirrors; and M, mirrors.

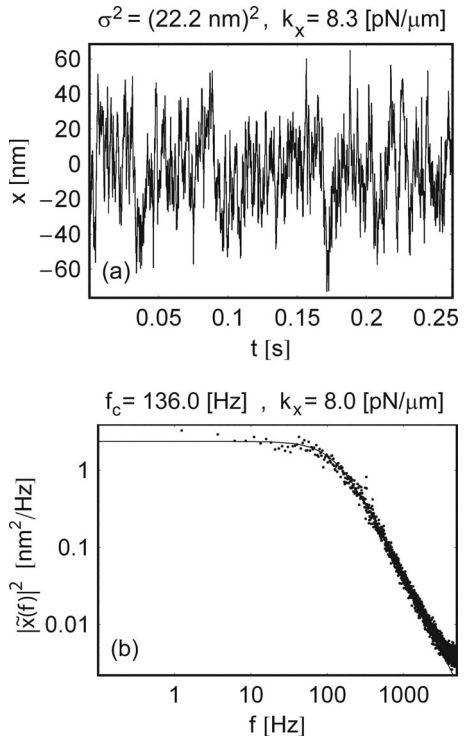

Fig. 4. Example of the experimental data used for trap stiffness measurements. (a) Time series data of suppressed Brownian motion of a 1 μm dye-doped polystyrene sphere in the optical trap at the wavelength of 810 nm at 28 mW. The trap stiffness is obtained using the standard deviation of the data and equipartition theorem. (b) The power spectrum of the Brownian motion data in (a). The trap stiffness is obtained from the corner frequency, f_c, of the spectrum, which in this case is f_c=136.0 Hz.

power spectrum of the particle's suppressed Brownian motion in the trap [Fig. 4(b)] as described in detail in [13,33,38]. For example, in Fig. 4(a) the variance of the particle's displacement, $\sigma^2=(22.2\ \mathrm{nm})^2$, yielded the trap stiffness, k_x=8.3 pN/μm, using the equipartition theorem,

$$\frac{1}{2}k_x\sigma^2=\frac{1}{2}k_BT, \tag{8}$$

where k_B is the Boltzmann constant and T is the temperature. The power spectrum of the position fluctuations [Fig. 4(b)] is given by [13]

$$|\tilde{x}(f)^2|=\frac{k_BT}{\pi^2\beta(f_c^2+f^2)}, \tag{9}$$

where f is the frequency, β is the drag coefficient of the particle in water, and f_c is the corner frequency, which is proportional to the trap stiffness, $f_c=k_x/(2\pi\beta)$. The data in Fig. 4(b) yielded a corner frequency of 136 Hz and a spring stiffness of k_x=8.0 pN/μm. A criterion for a reliable determination of the trap stiffness was that the three data analysis methods yielded similar values of k_x (within 10%–15%). Experimental controls, including measurements of the sphere-to-sphere and sample-to-sample variations of the trap stiffness, using our experimental procedures were conducted, and an experimental uncertainty of approximately 15% was determined. The linear dependence of the trap stiffness on the trapping laser power was also verified for both dye-doped and transparent spheres.

The trapping was done at a distance of approximately 16 μm from the coverslip inside the sample to avoid hydrodynamic effects near the coverslip surface. Particles were typically trapped at laser powers between 8 and 48 mW as measured after the dichroic mirror D2 and before the microscope objective (Fig. 3). To reduce the experimental uncertainty, measurements at each wavelength were performed on two to three spheres, with multiple data sets taken for each trapped sphere. The trap stiffness measurements at each wavelength were then averaged. Under the same experimental conditions, measurements on 1 μm transparent polystyrene spheres were also taken at each wavelength. The data from the dye-doped spheres were then normalized using the data from the transparent spheres. This was done to eliminate possible changes in the trapping force that may have resulted from slight variations in the incident laser beam characteristics upon adjusting the wavelength, any wavelength dependence of the optics, etc.

4. RESULTS AND DISCUSSION

A. Experimental

Figure 5 shows the transverse trap stiffness values (k_x-dyed), measured for the 625, 775, and 840 nm spheres normalized by those obtained for the transparent spheres (k_x-transparent). An enhancement in the trap stiffness, as presented, is a value of k_x-dyed/k_x-transparent greater than 1. Measurements for the 625 nm spheres were taken at wavelengths between 740 and 840 nm, which are on the red side of resonance. These results show that the 625 nm spheres could be trapped stably (i.e., trapped indefinitely long in three dimensions) at all wavelengths, and no significant change in the trap stiffness was observed as a function of wavelength. For the 775 nm spheres, mea-

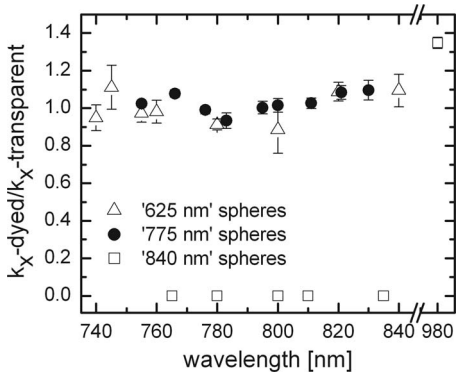

Fig. 5. Experimental results for the measurements of the trap stiffness near resonance. The wavelength dependence of the trap stiffness values (k dyed) is shown for 625, 775, and 840 nm dye-doped polystyrene spheres, all normalized by those measured on transparent spheres (k transparent) under the same conditions. An enhancement in the trap stiffness is a value greater than 1. For the 625 and 775 nm spheres, variations of the trap stiffness were within ~10% near resonance, which was within our experimental uncertainty. For the 840 nm spheres, a large effect due to the dye was observed, as no stable trapping could be achieved at 750–840 nm, but at 980 nm stable trapping was observed with a trap stiffness enhancement of ~35%.

surements were taken at wavelengths between 755 (on the blue side of resonance) and 840 nm (on the red side of resonance). For these particles, stable trapping was also possible at all wavelengths, with no significant difference between trap stiffness values at wavelengths on either side of resonance. For the 840 nm spheres we measured the trap strength on the red side of resonance at 980 nm, finding a small ~35% increase in the trap stiffness. However, the 840 nm spheres could not be stably trapped at wavelengths between 750 and 840 nm, which are on the blue side of resonance. At these wavelengths they could be trapped momentarily (~10 s) before diffusing from the trap. When stable trapping was not observed the trap stiffness was considered to be $k_x=0$ in Fig. 5. It can be seen from the data that there was little enhancement in the trap stiffness observed experimentally for the 625, 775, and 840 nm spheres, with an ~35% increase in the trap stiffness for the 840 nm spheres observed at a wavelength of 980 nm, and a ~10% increase for both the 625 and 775 nm spheres (which is within our experimental uncertainty).

B. Numerical Simulations

To aid in the explanation of these experimental results and to obtain further insight, we modeled the optical properties of our dye-doped spheres and calculated the force acting on them in an optical tweezer trap. In particular, we calculated the trap stiffness of both dye-doped and transparent polystyrene spheres in an optical trap at multiple wavelengths near resonance using software developed by Nieminen *et al.* [23]. The program implements the *T*-matrix formalism numerically, as described in Subsection 2.A, to calculate the trapping force, from which the trap stiffness can be determined by using $\boldsymbol{F_{trap}} = F_{trap\ x}\hat{\boldsymbol{x}} + F_{trap\ y}\hat{\boldsymbol{y}} + F_{trap\ z}\hat{\boldsymbol{z}} = -k_x x\hat{\boldsymbol{x}} - k_y y\hat{\boldsymbol{y}} - k_z z\hat{\boldsymbol{z}}$. Numerical results for the trap stiffness and for the dimensionless trap efficiency Q in the x and z directions are presented in this section. The trap efficiency is related to the trapping force by $F_{trap\ i} = n_m P Q_i / c$, where P is the laser power.

To model the complex index of refraction of the dye-doped polystyrene spheres, we obtained values of the molar extinction coefficient (from the manufacturer) for the dye in the spheres as a function of wavelength. The imaginary part of the index of refraction, κ, was then determined by using the molar extinction coefficient data, the molecular weight of the dye, the percentage dye loading of the sphere, the density of polystyrene, and the assumption that the dye was uniformly distributed in the sphere. The wavelength dependence of the extinction coefficient κ was then fit using the classic electron oscillator model of the complex dielectric constant [29],

$$\mathrm{Re}[\tilde{\varepsilon}(\omega)/\varepsilon_o] = \varepsilon_b + \sum_i f_i \frac{\omega_i^2 - \omega^2}{(\omega_i^2 - \omega^2)^2 + (\gamma_i \omega)^2}, \tag{10}$$

$$\mathrm{Im}[\tilde{\varepsilon}(\omega)/\varepsilon_o] = \sum_i f_i \frac{\gamma_i \omega}{(\omega_i^2 - \omega^2)^2 + (\gamma_i \omega)^2}, \tag{11}$$

and the relationship between the complex dielectric constant and the complex index of refraction,

$$\tilde{n}(\omega) = n(\omega) + i\kappa(\omega) = \sqrt{\tilde{\varepsilon}(\omega)/\varepsilon_o}, \tag{12}$$

where ε_b is the relative dielectric constant of the transparent polystyrene sphere ($\varepsilon_b=2.53$), ω_i are resonant frequencies, γ_i are the damping coefficients, and f_i are scaling variables that are proportional to the molecular density and oscillator strength of the resonances. For the fit of κ [Fig. 6(a)] we assumed two resonance frequencies ($i=1,2$). The 775 nm spheres have a peak value of $\kappa_{\mathrm{peak}}=0.054$. The refractive index n was then obtained using the fit parameters, f_i, γ_i, and Eqs. (10)–(12) as shown in Fig. 6(b). A similar analysis performed for the 840 nm spheres yielded a peak value of $\kappa_{\mathrm{peak}}=0.106$.

To calculate the trap stiffness for the model of the 775 nm dye-doped polystyrene spheres we first calculated the trap efficiency Q as a function of position in the trap. Example calculations of Q for the 775 nm dye-doped sphere as a function of position, at two trap wavelengths, are shown in Fig. 7. Simulations were performed using values from our experiments of $n_m=1.33$ and NA=1.25. Overfilling of the back aperture of the objective was not accounted for in the calculations (i.e., the Gaussian beam was not truncated). The geometry within the trap is shown in the inset of Fig. 7(a), with the origin of the coordinate system located at the focus of the trap. The trap efficiency Q_z (i.e., in the direction of laser propagation) as a function of position z is shown in Fig. 7(a) for wavelengths where both stable trapping occurs ($\lambda=596$ nm) and stable trapping is not possible ($\lambda=641$ nm). For

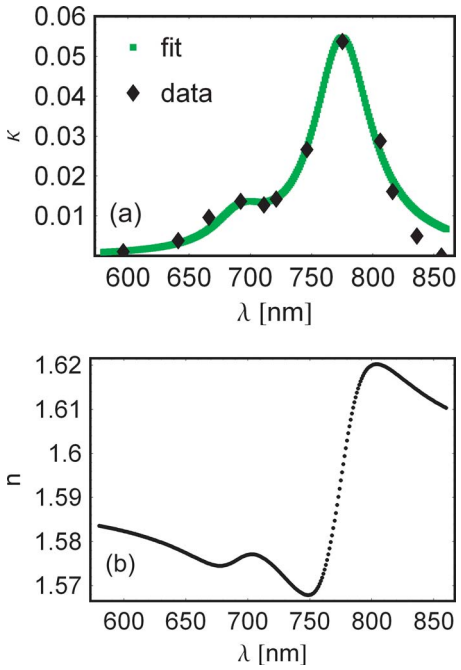

Fig. 6. (Color online) Wavelength dependence of the (a) imaginary and (b) real parts of the complex index of refraction, calculated by applying the classic electron oscillator model to the case of the 775 nm spheres used in our experiments. (a) Values for the imaginary part of the index of refraction, κ, obtained from the manufacturer of the dye in the 775 nm spheres (diamonds), fit using the classic electron oscillator model of the dielectric constant (curve). (b) The corresponding refractive index values n calculated using the parameters extracted from the fit of the κ values in (a) and Eqs. (10) and (12).

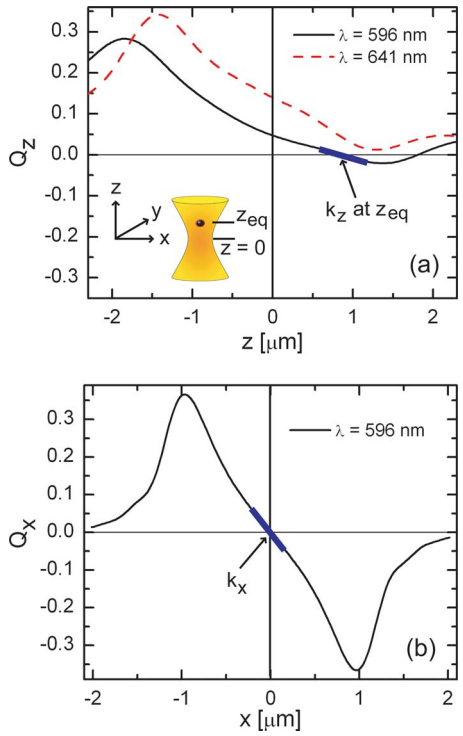

Fig. 7. (Color online) Numerically calculated trap efficiency Q in the (a) z direction (Q_z) and the (b) x direction (Q_x) as a function of position (z and x respectively) for the 775 nm spheres with $\kappa_{peak}=0.054$ and a diameter of 1 μm. The laser beam propagation is along the z axis, as indicated in the inset of (a). The trap stiffness k_z is determined from the slope of the $Q_z(z)$ at $z=z_{eq}$, as illustrated in (a) for the case of $\lambda=596$ nm. At $\lambda=641$ nm, stable trapping is not possible (i.e., z_{eq} is not achieved), and therefore in (b) the Q_x data are shown only for $\lambda=596$ nm. The trap stiffness k_x is calculated from the slope of $Q_x(x)$ at $x=0$ (i.e., in the center of the beam).

stable trapping to occur the magnitude of the gradient force must be larger than the scattering and absorption forces. When this is the case, the particle will find a stable equilibrium point at a positive z position in the trap (z_{eq}) where the trapping force in the z direction and Q_z are equal to zero. However, if the magnitude of the sum of the scattering and absorption forces is larger than the gradient force, then stable trapping in three dimensions is not possible, and there will be no equilibrium point for the particle in the trap. The trap efficiency in the transverse direction, Q_x, as a function of position x is shown in Fig. 7(b) for the same wavelengths. The calculations of Q_x are performed for the particle at its equilibrium position z_{eq}. In the case where stable trapping is not possible, Q_x is zero; hence no data are shown for $\lambda=641$ nm.

The trap stiffness k was calculated from the slope of the trap efficiency near the equilibrium positions in x and z, (i.e., $x=0$ and $z=z_{eq}$), as shown in Figs. 7(a) and 7(b). The calculated trap stiffness, k_x and k_z, for the 775 nm spheres normalized to k_x and k_z, respectively, for transparent spheres, at multiple wavelengths near resonance is shown in Fig. 8. It can be seen from the data that it is not possible to trap stably ($k_x=k_z=0$) near the resonance peak at wavelengths between 641 and 806 nm. This behavior near the peak absorption agrees with the experimental results for the 840 nm spheres (Fig. 4), but not for

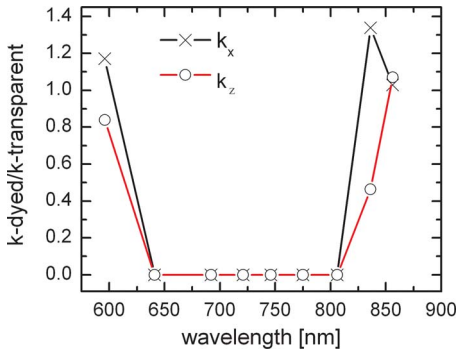

Fig. 8. (Color online) Numerically calculated wavelength dependence of the trap stiffness k_x and k_z for the 775 nm spheres with $\kappa_{peak}=0.054$ and a diameter of 1 μm (k-dyed), normalized by the corresponding values calculated for the 1 μm transparent polystyrene spheres (k-transparent). Stable trapping was not possible near resonance, which corresponds to zero values for k_x and k_z.

the 775 or 625 nm spheres. It can also be seen from Fig. 8 that at a wavelength of 836 nm (which is approximately 60 nm from the peak absorption) the simulations predict ~35% enhancement in k_x for the dye-doped spheres relative to the transparent spheres. However, at this wavelength the trap stiffness k_z is reduced so that the strength of the trap in three dimensions is not enhanced. At a trap wavelength of 856 nm (~80 nm from the wavelength of peak absorption), there is a less than 10% enhancement in the normalized trap stiffness in the x and z directions. Qualitatively, we expected the increase in the normalized trap stiffness at these wavelengths to be due in part to the increase in the refractive index off resonance [Fig. 6(b)]. In our model, the increase in refractive index is from 1.59 for the transparent spheres to 1.6145 at 836 nm and 1.6109 at 856 nm for the dye-doped 775 nm spheres. Interestingly, the simulations predict an enhancement in k_x of ~17% on the blue side of resonance at a wavelength of 641 nm as can be seen in Fig. 8. This is qualitatively unexpected given the reduction in the refractive index (1.5786) and the small amount of absorption ($\kappa=0.0038$) at this wavelength. Both of these would be expected to reduce the trap stiffness of the dye-doped spheres relative to the transparent spheres as is the case for k_z. It is possible, however, that Mie resonances in the EM fields [16,30], which are dependent on the ratio of the sphere diameter to the wavelength of light, might account for this behavior. The results from the simulations of the 775 nm 1 μm polystyrene spheres predict that the resonance of the dye does not provide a significant enhancement in the trap stiffness at wavelengths on the red side of resonance.

To gain insight as to why significant changes in the trap stiffness were not observed due to the resonance of the dye in the polystyrene, we performed simulations of the trap stiffness for nonabsorbing ("transparent") spheres with different refractive indices. The results of the simulations for k_x and k_z as functions of the relative refractive index m at a trap wavelength of 780 nm are shown in Fig. 9. Simulations were conducted for 1 μm ($d\sim\lambda$) and 20 nm ($d\ll\lambda$) spheres. It can be seen from the data that in both cases the trap stiffness increases almost linearly for small values of m, but for the 1 μm spheres

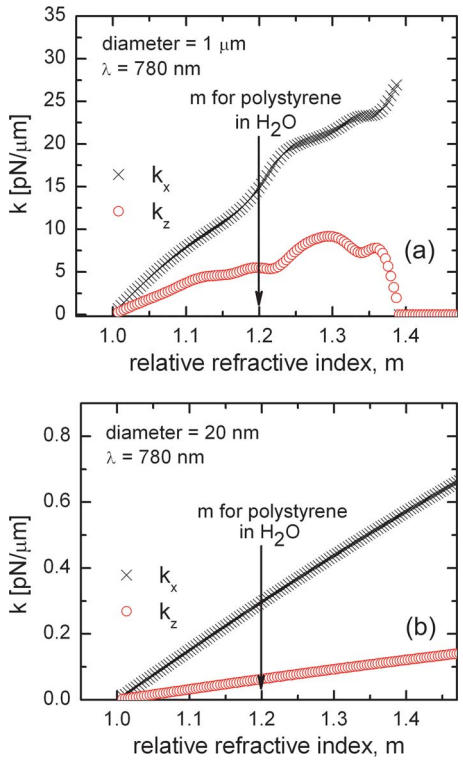

Fig. 9. (Color online) Numerically calculated dependence of the trap stiffness k_x and k_z, on the relative refractive index m for nonabsorbing (transparent) spheres with diameters of (a) 1 μm and (b) 20 nm, trapped at $\lambda=780$ nm. At $m>1.39$, stable trapping is not possible at this wavelength for 1 μm spheres ($k_z=0$) in (a), but is possible for 20 nm spheres in (b). Structure seen in (a) is due to Mie resonances.

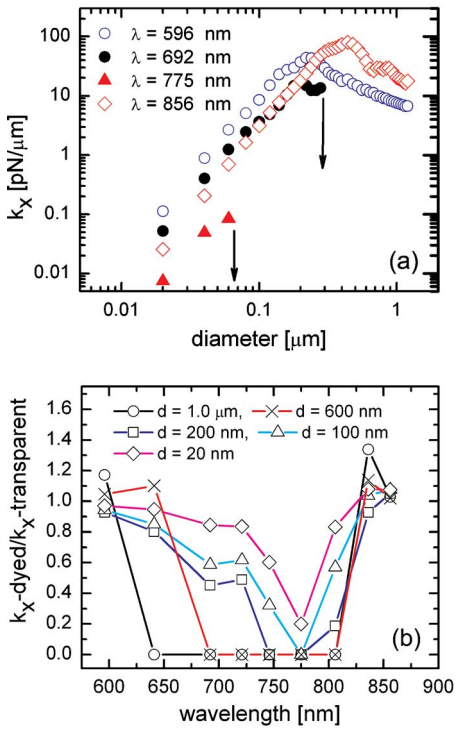

Fig. 10. (Color online) (a) Numerically calculated sphere diameter dependence of the trap stiffness k_x for the 775 nm spheres ($\kappa_{peak}=0.054$). Results are shown for several wavelengths near the resonance. At small sphere sizes, the trap stiffness increases with the diameter (d) as $k_x \sim d^3$, as expected for Rayleigh particles. At $\lambda=775$ nm (692 nm), stable trapping cannot be achieved for spheres larger than 60 nm (300 nm). (b) Numerically calculated wavelength dependence of the trap stiffness for the 775 nm spheres with $\kappa_{peak}=0.054$ (k_x-dyed), normalized by the corresponding values calculated for transparent polystyrene spheres (k_x-transparent). Results are shown for various sphere diameters. At the diameter of 20 nm, stable trapping is possible at all wavelengths near the resonance, which is not the case for larger spheres. The largest enhancement of ~35% is achieved in 1 μm spheres at $\lambda=836$ nm.

the existence of Mie scattering and resonances result in nonmonotonic behavior for larger m [39]. In addition, for larger values of m ($m>1.39$) the scattering from the sphere increases, thus increasing the scattering force and preventing stable trapping [Fig. 9(a)] [25]. This behavior does not occur for smaller particles (Rayleigh particles), because scattering is much smaller [Fig. 9(b)]. It can also be seen from Fig. 9(a) that an increase in the relative refractive index from $m=1.59/1.33=1.20$ (polystyrene in water) to $m=1.62/1.33=1.22$ [the maximum value of n from our model in Fig. 6(b)] results in an approximate increase in k_x of only ~20%. Thus the relative increase in the refractive index n resulting from the dye in the sphere is not substantial enough to provide a large increase in the trap stiffness.

To explore the effect of a dye resonance in nanometer-sized polystyrene spheres, we used our model for the 775 nm dye-doped spheres to explore the change in the trapping stiffness near resonance for smaller spheres. Figure 10(a) shows the trap stiffness k_x as a function of sphere diameter, at multiple trapping wavelengths. The numerical data show that stable trapping can be achieved at all wavelengths near resonance for particles smaller than 60 nm in diameter. Figure 10(b) shows normalized values of the trap stiffness k_x at wavelengths near resonance for particles 20 nm, 100 nm, 200 nm, 600 nm, and 1 μm in diameter. It can be seen from these results that it is possible to trap smaller particles near resonance and that there is a smaller reduction in the trap stiffness k_x on resonance. Similar results were obtained for the trap stiffness k_z (not shown). This is likely due to a decrease in the scattering and absorption cross sections as the particle becomes smaller. The results also show that the largest enhancement in the trap stiffness k_x occurred for the 1 μm diameter spheres (~35% at 836 nm). Reducing the sphere size did not produce an additional enhancement in the trap stiffness.

To further explore the effect of absorption from the dye on the trap stiffness, we changed the strength of absorption in our model of the 1 μm diameter 775 nm dye-doped spheres by scaling the extinction coefficient values κ. The values of κ in Fig. 5(a) were scaled to 150%, 25%, 10%, and 5% of the original values, resulting in peak values κ_{peak} of 0.081, 0.0135, 0.0054, and 0.0027, respectively. For each of the κ_{peak} values above, the scaled extinction coefficient as a function of wavelength was fit using the classic electron oscillator model, and new refractive index values were obtained. Figure 11 shows the results for the normalized trap stiffness k_x for the scaled extinction values. It can be seen that when the values of κ are reduced to 10% of their original values ($\kappa_{peak}=0.0054$) it is possible to trap at wavelengths on resonance, except for at the

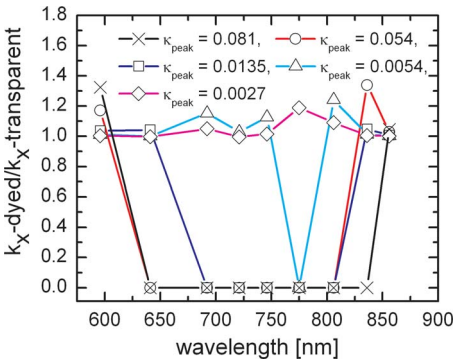

Fig. 11. (Color online) Numerically calculated wavelength dependence of the trap stiffness for the 775 nm spheres with a diameter of 1 μm (k_x-dyed), normalized by the corresponding values calculated for 1 μm transparent polystyrene spheres (k_x-transparent). Results are shown for different peak values of the extinction coefficient (κ_{peak}). Stable trapping is not possible for the larger values of the extinction coefficient. The largest enhancement of ~35% on the red side of the resonance occurs for $\kappa_{peak}=0.054$.

peak absorption ($\lambda=775$ nm). In addition, the reduction in absorption results in a reduction in the increase in the relative trap stiffness seen on the blue side of resonance at $\lambda=596$ nm, as compared with the increase at full absorption ($\kappa_{peak}=0.054$). When further reducing the absorption to 5% it becomes possible to trap at all wavelengths near resonance, which agrees with experimental results for the 625 and 775 nm spheres. It can also be seen from Fig. 11 that when the absorption is further reduced the enhancement of the trap stiffness on the red side of resonance is also reduced and that the maximum enhancement of ~35% occurs at $\kappa_{peak}=0.054$.

5. CONCLUSION

We explored, experimentally and numerically, the enhancement of the optical tweezer trapping force resulting from an optical resonance, using polystyrene spheres doped with dye as a model system. In both our experiments and numerical simulations we determined the trap stiffness at multiple trap wavelengths near the resonance. In our experimental and numerical results for dye-doped 1 μm spheres ($d\sim\lambda$), we did not find a substantial change or enhancement in the force at wavelengths near resonance when compared with polystyrene spheres without dye. Our numerical simulations also showed that a significant increase in the trap stiffness is not predicted for the dye-doped spheres if the size of the spheres is changed ($20\text{ nm}<d<1$ μm) or if the strength of the absorption ($0.0027<\kappa_{peak}<0.081$) of the dye is changed. In particular, the largest enhancement of the trap stiffness observed both experimentally and numerically was approximately 35%. The model could be further improved to include possible effects of nonuniform dye distribution in the sphere, which could be the cause of higher trap stiffness observed experimentally than that predicted theoretically for the same absorption strength near the resonance in 775 nm spheres. Nevertheless, we conclude that the optical resonance of a dye-doped polystyrene sphere (ranging in size from 20 nm to 1 μm) does not provide a significant enhancement of the optical tweezer trapping force.

ACKNOWLEDGMENTS

We thank T. A. Nieminen for the optical tweezers computational toolbox. This research was supported in part by the Office of Naval Research (ONR) via Oregon Nanoscience and Microtechnologies Institute (ONAMI) Nanometrology and Nanoelectronics Initiative (grant N00014-07-1-0457).

REFERENCES

1. A. Ashkin, "History of optical trapping and manipulation of small-neutral particle, atoms, and molecules," IEEE J. Sel. Top. Quantum Electron. **6**, 841–856 (2000).
2. M. D. Wang, H. Yin, R. Landick, J. Gelles, and S. M. Block, "Stretching DNA with optical tweezers," Biophys. J. **72**, 1335–1346 (1997).
3. K. Svoboda, C. F. Schmidt, B. J. Schnapp, and S. M. Block, "Direct observation of kinesin stepping by optical trapping interferometry," Nature **365**, 721–727 (1993).
4. E. R. Dufresne, G. C. Spalding, M. T. Dearing, S. A. Sheets, and D. G. Grier, "Computer-generated holographic optical tweezer arrays," Rev. Sci. Instrum. **72**, 1810–1816 (2001).
5. A. Ashkin, J. M. Dziedzic, J. E. Bjorkholm, and S. Chu, "Observation of a single-beam gradient force optical trap for dielectric particles," Opt. Lett. **11**, 288–290 (1986).
6. K. Svoboda and S. M. Block, "Optical trapping of metallic Rayleigh particles," Opt. Lett. **19**, 930–932 (1994).
7. S. Chu, J. E. Bjorkholm, A. Ashkin, and A. Cable, "Experimental-observation of optically trapped atoms," Phys. Rev. Lett. **57**, 314–317 (1986).
8. S. Schultz, D. R. Smith, J. J. Mock, and D. A. Schultz, "Single-target molecule detection with nonbleaching multicolor optical immunolabels," Proc. Natl. Acad. Sci. U.S.A. **97**, 996–1001 (2000).
9. M. Z. Liu, P. Guyot-Sionnest, T. W. Lee, and S. K. Gray, "Optical properties of rodlike and bipyramidal gold nanoparticles from three-dimensional computations," Phys. Rev. B **76**, 235428 (2007).
10. S. J. Oldenburg, J. B. Jackson, S. L. Westcott, and N. J. Halas, "Infrared extinction properties of gold nanoshells," Appl. Phys. Lett. **75**, 2897–2899 (1999).
11. A. D. Yoffe, "Semiconductor quantum dots and related systems: electronic, optical, luminescence and related properties of low dimensional systems," Adv. Phys. **50**, 1–208 (2001).
12. H. Kataura, Y. Kumazawa, Y. Maniwa, I. Umezu, S. Suzuki, Y. Ohtsuka, and Y. Achiba, "Optical properties of single-wall carbon nanotubes," Synth. Met. **103**, 2555–2558 (1999).
13. K. C. Neuman and S. M. Block, "Optical trapping," Rev. Sci. Instrum. **75**, 2787–2809 (2004).
14. C. Selhuber-Unkel, I. Zins, O. Schubert, C. Sonnichsen, and L. B. Oddershede, "Quantitative optical trapping of single gold nanorods," Nano Lett. **8**, 2998–3003 (2008).
15. G. Mie, "Beiträge Zur Optik Trüber Medien, Speziell Kolloidaler Metallösungen," Ann. Phys. (Leipzig) **25**, 377–445 (1908).
16. H. C. d. Hulst, *Light Scattering by Small Particles*, 1st ed. (Dover, 1981).
17. M. I. Mishchenko, L. D. Travis, and A. A. Lacis, *Scattering, Absorption, and Emission of Light by Small Paticles*, 1st ed. (Cambridge U. Press, 2002).
18. K. F. Ren, G. Grehan, and G. Gouesbet, "Radiation pressure forces exerted on a particle arbitrarily located in a Gaussian-beam by using the generalized Lorenz–Mie

theory, and associated resonance effects," Opt. Commun. **108**, 343–354 (1994).
19. T. A. Nieminen, H. Rubinsztein-Dunlop, N. R. Heckenberg, and A. I. Bishop, "Numerical modelling of optical trapping," Comput. Phys. Commun. **142**, 468–471 (2001).
20. T. A. Nieminen, H. Rubinsztein-Dunlop, and N. R. Heckenberg, "Multipole expansion of strongly focused laser beams," J. Quant. Spectrosc. Radiat. Transf. **79–80**, 1005–1017 (2003).
21. T. A. Nieminen, H. Rubinsztein-Dunlop, and N. R. Heckenberg, "Calculation of the T-matrix: general considerations and application of the point-matching method," J. Quant. Spectrosc. Radiat. Transf. **79–80**, 1019–1029 (2003).
22. T. A. Nieminen, N. R. Heckenberg, and H. Rubinsztein-Dunlop, "Computational modelling of optical tweezers," Proc. SPIE **5514**, 514–523 (2004).
23. T. A. Nieminen, V. L. Y. Loke, A. B. Stilgoe, G. Knöner, A. M. Branczyk, N. R. Heckenberg, and H. Rubinsztein-Dunlop, "Optical tweezers computational toolbox," J. Opt. A, Pure Appl. Opt. **9**, S196–S203 (2007).
24. C. H. Choi, J. Ivanic, M. S. Gordon, and K. Ruedenberg, "Rapid and stable determination of rotation matrices between spherical harmonics by direct recursion," J. Chem. Phys. **111**, 8825–8831 (1999).
25. A. Ashkin, "Forces of a single-beam gradient laser trap on a dielectric sphere in the ray optics regime," Biophys. J. **61**, 569–582 (1992).
26. N. Malagnino, G. Pesce, A. Sasso, and E. Arimondo, "Measurements of trapping efficiency and stiffness in optical tweezers," Opt. Commun. **214**, 15–24 (2002).
27. M. Born and E. Wolf, *Principles of Optics*, 7th ed. (Cambridge U. Press, 2005).
28. L. Novotny and B. Hect, *Principles of Nano-Optics*, 1st ed. (Cambridge U. Press, 2006).
29. J. D. Jackson, *Classical Electrodynamics*, 3rd ed. (Wiley, 1998).
30. C. F. Bohren and D. R. Huffman, *Absorption and Scattering of Light by Small Particles*, 1st ed. (Wiley, 1998).
31. D. T. Chiu and R. N. Zare, "Biased diffusion, optical trapping, and manipulation of single molecules in solution," J. Am. Chem. Soc. **118**, 6512–6513 (1996).
32. K. C. Toussaint, M. Liu, M. Pelton, J. Pesic, M. J. Guffey, P. Guyot-Sionnest, and N. F. Scherer, "Plasmon resonance-based optical trapping of single and multiple Au nanoparticles," Opt. Express **15**, 12017–12029 (2007).
33. P. M. Hansen, V. K. Bhatia, N. Harrit, and L. Oddershede, "Expanding the optical trapping range of gold nanoparticles," Nano Lett. **5**, 1937–1942 (2005).
34. R. R. Agayan, F. Gittes, R. Kopelman, and C. F. Schmidt, "Optical trapping near resonance absorption," Appl. Opt. **41**, 2318–2327 (2002).
35. M. J. Lang, P. M. Fordyce, A. M. Engh, K. C. Neuman, and S. M. Block, "Simultaneous, coincident optical trapping and single-molecule fluorescence," Nat. Methods **1**, 133–139 (2004).
36. K. Svoboda and S. M. Block, "Biological applications of optical forces," Annu. Rev. Biophys. Biomol. Struct. **23**, 247–285 (1994).
37. K. Visscher, S. P. Gross, and S. M. Block, "Construction of multiple-beam optical traps with nanometer-resolution position sensing," IEEE J. Sel. Top. Quantum Electron. **2**, 1066–1076 (1996).
38. L. Oddershede, S. Grego, S. F. Nørrelykke, and K. Berg-Sørensen, "Optical tweezers: probing biological surfaces," Probe Microsc. **2**, 129–137 (2001).
39. G. Knöner, S. Parkin, T. A. Nieminen, N. R. Heckenberg, and H. Rubinsztein-Dunlop, "Measurement of the index of refraction of single microparticles," Phys. Rev. Lett. **97**, 157402 (2006).